https://doi.org/10.5194/wes-2026-128
Preprint. Discussion started: 17 August 2026

Adaptive multi-mode unity-magnitude input shaping with unknown-input state estimation for floating offshore wind turbines

Amina Mseddi[1], Imed Bouzida[2,3], and Omar Naifar[1,4]

[1]Control and Energy Management Laboratory (CEM-Lab), National School of Engineering of Sfax, University of Sfax, Sfax, Tunisia
[2]Abu Dhabi University, Abu Dhabi, United Arab Emirates
[3]Laboratory of Probability and Statistics, University of Sfax, Sfax, Tunisia
[4]Higher Institute of Applied Science and Technology of Kairouan, University of Kairouan, Kairouan, Tunisia

Correspondence: Amina Mseddi (amina.mseddi@enis.tn)

Abstract. Every operational transition of a floating offshore wind turbine (FOWT) — a start-up, a curtailment change, a grid-support set-point, a change of operating region — moves a control set-point and thereby injects energy into the lightly damped structural modes. Input shaping removes that command-induced excitation by construction, but it is a feedforward mechanism whose guarantees are exact only for a known modal model. This paper gives a complete and verifiable treatment of an adaptive multi-mode unity-magnitude (UM) shaping layer supported by an unknown-input observer, on a coupled control-oriented FOWT model in which the structural motion feeds back into the rotor aerodynamics. Four results are proved: convolving single-mode UM shapers cancels every targeted mode exactly; a non-asymptotic bound limits the residual under amplitude and timing perturbation; the same bound maps a modal-frequency estimation error into a residual bound; and rescaling the impulse instants by the estimated damped frequency preserves cancellation exactly at fixed damping. The estimation layer is placed on a firm footing by an observability analysis and a full-order unknown-input observer with proved decoupled convergence. The numerical study — run on the coupled model, with a second-order pitch actuator, rate and saturation limits, timing quantization, and independent per-mode drift — yields a design result that a decoupled model conceals: because collective pitch strongly damps the platform mode ($\zeta = 0.32$), shaping it is counterproductive. Dropping it gives a shaper that is $9\times$ shorter ($0.86\,\mathrm{s}$ versus $7.86\,\mathrm{s}$, 9 versus 27 impulses), reduces the command-induced tower damage-equivalent load by $51.4\,\%$ instead of $29.8\,\%$, lowers rather than raises the peak tower deflection, and cuts the out-of-band spillover from 19.2 to 6.9. The recommendation is therefore to shape the lightly damped modes and let aerodynamics damp the platform. All model matrices, shaper instants, and observer gains are given so that the study can be reproduced.

Keywords. floating offshore wind turbine; input shaping; unity-magnitude shaper; multi-mode cancellation; unknown-input observer; command-induced fatigue; reduced-order modelling

1 Introduction

Floating offshore wind turbines carry lightly damped, low-frequency structural modes on a compliant support, and their modal parameters drift with sea state, ballast, water depth and operating point (Jonkman and Matha, 2011; Bai et al., 2026). Most control research on these machines addresses *disturbance rejection*: how feedback should respond to turbulent wind and irregular waves. Robust and model-based designs have been proposed for that purpose, including linear-quadratic and resonant schemes, individual-pitch control, and economic nonlinear model-predictive control (Hawari et al., 2023; Pustina et al., 2020, 2023, 2025; Liu et al., 2025; Hummel et al., 2025; Aslmostafa et al., 2026), alongside the open-source reference controller ROSCO (Abbas et al., 2022). A pitch-controlled floating turbine can even feed energy back into the platform motion if the loop phase is wrong (Larsen and Hanson, 2007).

A different and complementary source of structural load has received far less attention: the turbine's own *commands*. A FOWT does not sit at one set-point. It starts up and shuts down, it is curtailed and de-rated, it answers grid-support requests, it changes operating region, and it recovers from faults. Every such transition moves a set-point, and a set-point that moves carelessly rings the structure. This excitation is not a disturbance to be rejected; it is self-inflicted and can be removed *before* it enters the plant.

Input shaping does exactly that. Convolving a command with a short impulse sequence places zeros of the command spectrum on the flexible poles, so the command cannot excite them (Singer and Seering, 1990; Singhose, 2009). The unity-magnitude (UM) variant restricts the impulses to ± 1, which suits a fast command channel and gives a short sequence (Gürleyük, 2006). Shaping has been extended to explicit fractional-derivative descriptions and to real-time synthesis (Abid et al., 2016; Poty et al., 2003; Alshaya, 2025; Mseddi et al., 2024). Its limitation is equally clear and we state it plainly: shaping is feed-forward, it cannot reject unmeasured disturbances, and its cancellation is exact only for a modal model that is known. That is precisely why an estimation layer, and a quantified account of what happens when the model is wrong, are needed.

This paper supplies both, and does so on a model in which the coupling that defines a FOWT is present: the wind seen by the rotor depends on the structural motion, so tower and platform velocities feed back into the aerodynamic torque and thrust. Working on such a model, rather than on separate drivetrain and structural subsystems, turns out to change the engineering conclusion. The contributions are: (i) a proof that convolving single-mode UM shapers cancels every targeted mode exactly (Theorem 3.1); (ii) a non-asymptotic residual bound under amplitude and timing perturbation (Proposition 3.3), together with its specialization to modal-frequency estimation error (Corollary 3.5); (iii) a proof that rescaling the impulse instants by the estimated damped frequency preserves cancellation exactly at fixed damping (Theorem 3.7); (iv) an observability analysis and an unknown-input observer with proved decoupled convergence (Theorem 3.9); and (v) an actuator-aware numerical study which shows that the platform mode — strongly damped by collective pitch — should be excluded from the shaper, giving a shorter shaper that performs better on every metric that matters.

We are explicit about scope. The study is carried out on a seven-state control-oriented model; it is a verification of the stated mechanisms and a design study, not turbine-level evidence. Section 5 states the limitations, and high-fidelity cross-validation is identified as necessary further work.

https://doi.org/10.5194/wes-2026-128
Preprint. Discussion started: 17 August 2026

2 Preliminaries and problem statement

55 This section states the model, recalls the residual-vibration functional, defines the shaper, and fixes the assumptions. Throughout, s is the Laplace variable, $j = \sqrt{-1}$, and $\|\cdot\|$ is the Euclidean norm.

Definition 2.1 (Coupled control-oriented FOWT model)**.** Let $x = [\theta_{dt}, \omega_r, \omega_g, q_{fa}, \dot{q}_{fa}, \theta_p, \dot{\theta}_p]^\top \in \mathbb{R}^7$ collect the drivetrain torsion angle, the rotor and generator speeds, the tower fore–aft deflection and its rate, and the platform-pitch angle and its rate. The wind seen by the rotor depends on the structural motion,

60 $$V_{\text{rel}} = V_w - \left(\dot{q}_{fa} + L_t\,\dot{\theta}_p\right), \tag{1}$$

with L_t the hub height above the platform reference, and both the aerodynamic torque and the thrust depend on the operating point through

$$\Delta T_a = g_\omega \Delta\omega_r + g_\beta \Delta\beta + g_V \Delta V_{\text{rel}}, \qquad \Delta F_t = k_\omega \Delta\omega_r + k_\beta \Delta\beta + k_V \Delta V_{\text{rel}}. \tag{2}$$

With the two-mass drivetrain, a tower fore–aft modal oscillator and a platform-pitch oscillator driven by ΔF_t at the arm L_t,
65 the linearized dynamics about an above-rated operating point are

$$\dot{x} = Ax + Bu + Ed, \qquad y = Cx, \tag{3}$$

with $u = [T_g, \beta]^\top$ (generator torque, collective pitch) and $d = [V_w, M_{\text{wave}}]^\top$. Substituting Eqs. (1)–(2) makes A non-block-diagonal: every input reaches every output, and in particular $q_{fa}/T_g \neq 0$, $\theta_p/T_g \neq 0$ and $\omega_r/\beta \neq 0$. The numerical realization is given in Appendix B.

70 The retained modes are complex-conjugate pole pairs $s_k = -\zeta_k\omega_{n,k} \pm j\omega_{d,k}$, with $\omega_{d,k} = \omega_{n,k}\sqrt{1-\zeta_k^2}$, obtained as eigenvalues of the coupled A rather than imposed. We write $a_k \triangleq \zeta_k\omega_{n,k}$.

A shaper is a sequence of impulses $\{(A_i, t_i)\}_{i=1}^m$ convolved with a command; its Laplace transform is the quasi-polynomial

$$\hat{S}(s) = \sum_{i=1}^{m} A_i\, e^{-st_i}. \tag{4}$$

Lemma 2.2 (Residual vibration of a shaped command (Singer and Seering, 1990; Singhose, 2009))**.** *For a mode with pole*
75 *$s_k = -a_k + j\omega_{d,k}$, the residual-vibration amplitude left by $\{(A_i, t_i)\}$, normalized to that of a unit impulse, is*

$$V_k = \left|\hat{S}(s_k)\right| e^{-a_k t_m} = e^{-a_k t_m}\sqrt{\mathcal{C}_k^2 + \mathcal{S}_k^2}, \tag{5}$$

with $\mathcal{C}_k = \sum_i A_i e^{a_k t_i}\cos(\omega_{d,k} t_i)$, $\mathcal{S}_k = \sum_i A_i e^{a_k t_i}\sin(\omega_{d,k} t_i)$ and $t_m = \max_i t_i$. The shaper cancels mode k exactly if and only if $\hat{S}(s_k) = 0$, i.e. $\mathcal{C}_k = \mathcal{S}_k = 0$.

Definition 2.3 (Unity-magnitude shaper (Gürleyük, 2006))**.** A three-impulse UM shaper for one mode has amplitudes $A =$
80 $[+1, -1, +1]$ and instants $t = [0, t_2, t_3]$ chosen so that $\hat{S}(s_k) = 0$. The instants are computed in Appendix A.

https://doi.org/10.5194/wes-2026-128
Preprint. Discussion started: 17 August 2026

The assumptions are stated next. Assumption 1 removes the ambiguity about which signal is shaped, which is essential because the cancellation analysis depends on the transfer path from that signal to each structural output.

Assumption 1 (Shaped channel)**.** *The shaper is a feedforward pre-filter on the* collective-pitch supervisory set-point*:* $\beta_{\mathrm{cmd}} = S * r$*, where* r *is the set-point demanded by the supervisory logic. The relevant structural paths are therefore* q_{fa}/β *and* θ_p/β*, whose poles are the modes of Eq. (3). The shaper is not placed inside a feedback loop.*

Assumption 2 (Maneuver-time invariance)**.** *The modal parameters are constant over the duration of one shaped maneuver, and the shaper is updated only between maneuvers, so that a queued impulse sequence is executed with fixed instants.*

Assumption 3 (Measurements)**.** *The measured outputs are the rotor speed, the tower-top fore–aft velocity (obtained by integrating the tower-top accelerometer), and the platform-pitch angle and rate (from the platform inertial unit). Thus* $y = Cx$ *with* C *selecting these four states, and the unknown wave input does not feed through to the measurement.*

3 Main results

We now present the framework. The shaping layer removes the vibration that set-point transitions would otherwise inject into the structural modes: Theorem 3.1 establishes exact cancellation of every targeted mode, Proposition 3.3 bounds what remains when the impulses are perturbed, Corollary 3.5 converts a modal-frequency estimation error into such a bound, and Theorem 3.7 shows that a single scalar rescaling per mode restores exact cancellation under frequency drift. The estimation layer that supplies the modal information and the states is treated in Theorem 3.9.

Theorem 3.1. *For* $k = 1, \dots, N$ *let* S_k *be a single-mode UM shaper with* $\hat{S}_k(s_k) = 0$*, and let* $S = S_1 * S_2 * \cdots * S_N$*. Then*

$$V_\ell = 0, \qquad \ell = 1, \dots, N. \tag{6}$$

Proof. Convolution of impulse sequences multiplies their Laplace transforms. Each impulse of S has amplitude $\prod_k A^{(k)}$ and instant $\sum_k t^{(k)}$, and the exponential of a sum is the product of exponentials, so Eq. (4) factorizes,

$$\hat{S}(s) = \prod_{k=1}^{N} \hat{S}_k(s). \tag{7}$$

Fix a targeted mode ℓ and evaluate Eq. (7) at its pole,

$$\hat{S}(s_\ell) = \hat{S}_\ell(s_\ell) \prod_{k \neq \ell} \hat{S}_k(s_\ell). \tag{8}$$

By construction $\hat{S}_\ell(s_\ell) = 0$, hence $\hat{S}(s_\ell) = 0$. By Lemma 2.2 the residual of the convolved shaper at mode ℓ is

$$V_\ell = \left|\hat{S}(s_\ell)\right| e^{-a_\ell t_m} = 0, \tag{9}$$

and ℓ was arbitrary. □

https://doi.org/10.5194/wes-2026-128
Preprint. Discussion started: 17 August 2026

Remark 3.2. The construction preserves the commanded final value. Each single-mode UM sequence has $\sum_j A_j^{(k)} = 1$, and by Eq. (7) at $s = 0$, $\sum_i A_i = \prod_k \sum_j A_j^{(k)} = 1$, so the shaped command reaches the same set-point as the unshaped one; the synthesized shaper of Sect. 4 satisfies this to twelve digits. Theorem 3.1 is a formalization for the present architecture rather than a new principle: it follows from the convolution theorem and the single-mode zero condition, and its value here is that it reduces multi-mode design to N independent two-equation solves.

Proposition 3.3. *Let $S = \{(A_i, t_i)\}$ satisfy $\hat{S}(s_\ell) = 0$, and let $\tilde{S}$ have amplitudes $A_i + \delta A_i$ and instants $t_i + \delta t_i$, with $\tilde{t}_m = \max_i(t_i + \delta t_i)$. Then*

$$\tilde{V}_\ell \le e^{-a_\ell \tilde{t}_m} \sum_i e^{a_\ell t_i} \Big(|\delta A_i| + |A_i|\,\omega_{n,\ell}\,|\delta t_i| \Big)\, e^{\omega_{n,\ell}|\delta t_i|}. \tag{10}$$

Proof. Since $\hat{S}(s_\ell) = 0$, the perturbed transform at the pole is

$$\hat{\tilde{S}}(s_\ell) = \sum_i e^{-s_\ell t_i} \big[(A_i + \delta A_i) e^{-s_\ell \delta t_i} - A_i \big]. \tag{11}$$

Write the bracket as $\delta A_i\, e^{-s_\ell \delta t_i} + A_i \big(e^{-s_\ell \delta t_i} - 1\big)$. Apply $|e^z - 1| \le |z|\, e^{|z|}$ with $z = -s_\ell \delta t_i$, and use $|s_\ell| = \omega_{n,\ell}$,

$$\big|(A_i + \delta A_i) e^{-s_\ell \delta t_i} - A_i\big| \le \big(|\delta A_i| + |A_i|\,\omega_{n,\ell}|\delta t_i| \big) e^{\omega_{n,\ell}|\delta t_i|}. \tag{12}$$

Multiply by $|e^{-s_\ell t_i}| = e^{a_\ell t_i}$, sum over i, and apply Lemma 2.2 with the factor $e^{-a_\ell \tilde{t}_m}$ to obtain Eq. (10). □

Remark 3.4. Bound (10) is non-asymptotic: no term is discarded. It is, however, a worst-case triangle-inequality bound that ignores phasor cancellation between impulses, and Sect. 4 measures it to be 2.3 to 38 times larger than the actual residual. It should therefore be read as a certificate, not as a predictor. The weight $e^{a_\ell t_i}$ shows that late impulses acting on high-frequency modes are the expensive ones, which is why the drivetrain mode dominates the quantization error. Truncation is the case $\delta A_i = -A_i$; when two impulses are merged at a common instant, both sequences are first embedded in a common index set, padding with zero amplitudes, so that a merge is represented by one amplitude deletion and one timing perturbation.

Corollary 3.5. *Let the shaper be built on an estimated damped frequency $\hat{\omega}_{d,\ell} = \omega_{d,\ell}(1+\delta)$ at correct damping, so that the instants are $\hat{t}_i = \varphi_i / \hat{\omega}_{d,\ell}$. Then the timing error with respect to the exact instants $t_i = \varphi_i / \omega_{d,\ell}$ is*

$$\delta t_i = \hat{t}_i - t_i = -\frac{\delta}{1+\delta}\, t_i, \tag{13}$$

and the residual obeys Eq. (10) with $\delta A_i = 0$ and δt_i given by Eq. (13).

Proof. By definition $\hat{t}_i = \varphi_i / \hat{\omega}_{d,\ell} = \varphi_i / \big(\omega_{d,\ell}(1+\delta)\big) = t_i/(1+\delta)$. Subtracting t_i gives $\delta t_i = t_i\big(1/(1+\delta) - 1\big) = -\delta t_i/(1+\delta)$, which is Eq. (13). Substituting into Proposition 3.3 with unperturbed amplitudes gives the bound. □

Remark 3.6. Corollary 3.5 is what makes the identification requirement quantitative: it converts an accuracy specification on the modal estimator into a residual guarantee. Section 4 reports, for instance, that a $2\,\%$ frequency error leaves at most $6.5\,\%$ residual by the bound and $3.4\,\%$ in fact.

https://doi.org/10.5194/wes-2026-128
Preprint. Discussion started: 17 August 2026

Theorem 3.7. *Let a single-mode UM shaper be designed for* (ω_n, ζ) *with instants* t_i*, and let the natural frequency drift to* ω_n' *at fixed* ζ*. Then the rescaled shaper with instants*

$$t_i' = \frac{\omega_d}{\omega_d'} t_i, \qquad \omega_d' = \omega_n' \sqrt{1-\zeta^2}, \tag{14}$$

cancels the drifted mode exactly. Equivalently, the normalized instants $\varphi_i = \omega_d t_i$ *depend on* ζ *alone, so the ratios* t_i/t_j *are invariant under frequency drift.*

Proof. By Lemma 2.2 the cancellation conditions are $\mathcal{C} = \mathcal{S} = 0$ with

$$\mathcal{C} = \sum_i A_i e^{\zeta\omega_n t_i} \cos(\omega_d t_i), \qquad \mathcal{S} = \sum_i A_i e^{\zeta\omega_n t_i} \sin(\omega_d t_i). \tag{15}$$

Use $\zeta\omega_n t_i = \dfrac{\zeta}{\sqrt{1-\zeta^2}} \omega_d t_i$, so both sums depend on the instants only through $\omega_d t_i$. Introduce $\varphi_i = \omega_d t_i$, giving

$$\mathcal{C} = \sum_i A_i e^{\frac{\zeta}{\sqrt{1-\zeta^2}}\varphi_i} \cos\varphi_i, \qquad \mathcal{S} = \sum_i A_i e^{\frac{\zeta}{\sqrt{1-\zeta^2}}\varphi_i} \sin\varphi_i. \tag{16}$$

These contain ζ but not ω_n, so a solution $\{\varphi_i\}$ of $\mathcal{C} = \mathcal{S} = 0$ is a function of ζ alone. Apply the drift and the rescaling of Eq. (14), which gives $\omega_d' t_i' = \omega_d' \dfrac{\omega_d}{\omega_d'} t_i = \omega_d t_i = \varphi_i$. The normalized instants are unchanged, so $\mathcal{C} = \mathcal{S} = 0$ still holds at (ω_n', ζ), and by Lemma 2.2 the residual is zero. Finally, $t_i/t_j = \varphi_i/\varphi_j$ is independent of ω_n, which is the constant-ratio property. □

Remark 3.8. Theorem 3.7 reduces adaptation to one scalar per mode: only the current damped frequency is needed and the pre-computed ratios do the rest. It is exact for frequency drift at *fixed* damping and claims nothing more; when the damping also drifts, the normalized instants move and cancellation degrades, which Sect. 4 quantifies by Monte-Carlo ($0.00\,\%$ residual when ζ is exact, up to $6.0\,\%$ mean when ζ varies by $\pm 30\,\%$). Algorithm 1 implements the update between maneuvers, per Assumption 2, gated by the estimator confidence so that noisy estimates do not trigger retiming; a damping change is handled by a one-dimensional lookup $\varphi_i(\zeta)$ computed offline.

Theorem 3.9. *Consider Eq. (3) with the measurement matrix* C *of Assumption 3 (so* $y = Cx$*, no unknown-input feedthrough) and full-column-rank unknown-input matrix* E*. Suppose (a)* (A, C) *is observable; (b)* $\operatorname{rank}(CE) = \operatorname{rank}(E)$*; and (c) the pair* (TA, C) *with* $T = I - E(CE)^+C$ *is detectable. Then a gain* K_1 *exists making* $F = TA - K_1 C$ *Hurwitz, and the full-order observer*

$$\dot{z} = Fz + TBu + Ky, \qquad \hat{x} = z + Hy, \qquad H = E(CE)^+,\ K = K_1 + FH, \tag{17}$$

yields an estimation error $e = x - \hat{x}$ *that is decoupled from the unknown input and obeys* $\dot{e} = Fe$*, so* $e(t) \to 0$ *exponentially.*

Proof. Form the error $e = x - \hat{x} = x - z - Hy = (I - HC)x - z = Tx - z$. Differentiate and substitute Eqs. (3) and (17),

$$\dot{e} = T\dot{x} - \dot{z} = T(Ax + Bu + Ed) - \big(Fz + TBu + KCx\big). \tag{18}$$

https://doi.org/10.5194/wes-2026-128
Preprint. Discussion started: 17 August 2026

Algorithm 1 Between-maneuver update of the multi-mode UM shaper

Require: modal estimates $\{\hat{\omega}_{n,k}, \hat{\zeta}_k\}$ and confidences $\{\gamma_k\}$; offline maps $\varphi_i^{(k)}(\zeta)$

for each targeted lightly damped mode k **do**
    if $\gamma_k \le \bar{\gamma}$ **then** {confidence gate; $\gamma_k = \mathrm{tr}$ of the modal covariance}
        $\varphi_i^{(k)} \leftarrow \varphi_i^{(k)}(\hat{\zeta}_k)$ {damping via the offline map}
        $t_i^{(k)} \leftarrow \varphi_i^{(k)} / \left(\hat{\omega}_{n,k}\sqrt{1-\hat{\zeta}_k^2}\right)$ {frequency via Theorem 3.7}
    end if
end for
$S \leftarrow S_1 * \cdots * S_N$ {Theorem 3.1}
quantize the instants to the command grid Δt {error bounded by Proposition 3.3}
return S {frozen for the next maneuver (Assumption 2)}

The input term TBu cancels. Because E has full column rank q and $\mathrm{rank}(CE) = \mathrm{rank}(E) = q$, the matrix CE has full column rank, so $(CE)^+CE = I_q$; hence

$$TE = (I - HC)E = E - E(CE)^+CE = 0, \tag{19}$$

and the unknown input drops out. Writing $z = Tx - e$ and $y = Cx$ leaves

$$\dot{e} = TAx - F(Tx - e) - KCx = Fe + \Xi x, \qquad \Xi \triangleq TA - FT - KC. \tag{20}$$

Substitute $F = TA - K_1C$ and $K = K_1 + FH$, and use $I - T = HC$,

$$\Xi = TA - (TA - K_1C)T - (K_1 + FH)C = (TA - K_1C)(I - T) - FHC = (TA - K_1C - F)HC = 0, \tag{21}$$

because $F = TA - K_1C$. Hence $\dot{e} = Fe$, independent of d, and F Hurwitz gives exponential convergence; the existence of such a K_1 is exactly hypothesis (c). □

Remark 3.10. Theorem 3.9 is a standard full-order unknown-input observer (Darouach et al., 1994); it is included because the shaping layer needs states and modal information, and because the conditions under which it may be used are often left unstated. Condition (a) documents reconstructibility of the disturbance-free realization; the decoupling and convergence rest on (b) and (c), and (a) is in fact stronger than necessary once (c) holds. Conditions (a) and (c) are properties of the specific numerical realization, not consequences of the sensor list, and are verified in Sect. 4. The measurement set of Assumption 3 consists of state selections, so $y = Cx$ holds exactly; had a tower-top acceleration been used directly it would be a row of CA with disturbance feedthrough, requiring a modified construction, which is avoided here.

4 Numerical demonstration

The study uses the coupled seven-state model of Definition 2.1, whose parameters are representative of the IEA 15 MW turbine on the UMaine VolturnUS-S semi-submersible platform (Gaertner et al., 2020; Allen et al., 2020). It is a design-oriented model,

https://doi.org/10.5194/wes-2026-128
Preprint. Discussion started: 17 August 2026

Table 1. Settings of the numerical study.

Reference turbine / platform	IEA 15 MW / UMaine VolturnUS-S (parameters representative, not identified)
Rated rotor speed	$0.792\,\mathrm{rad\,s^{-1}}$ (7.56 rpm); hub arm $L_t = 150\,\mathrm{m}$
Shaped channel	collective-pitch supervisory set-point (Assumption 1)
Command grid	10 ms (also 2, 5, 20 ms in the quantization study)
Pitch actuator	2nd order, 1 Hz, $\zeta = 0.7$; rate limit $8^\circ\,\mathrm{s}^{-1}$; travel $\pm 30^\circ$
Maneuver sequence	pitch set-point steps at $t = 50, 140, 230, 320, 410, 500\,\mathrm{s}$
	of $+2.0, -1.5, +2.5, -2.0, +1.0, -2.0$ degrees
DEL	rainflow, Wöhler slope $m = 4$, $N_{\mathrm{eq}} = f_{\mathrm{eq}} T$ with $f_{\mathrm{eq}} = 1\,\mathrm{Hz}$,
	$T = 580\,\mathrm{s}$, first 20 s discarded, half-cycles weighted 0.5, no mean-stress
	correction, channels in N m
Monte-Carlo	400 samples; independent per-mode ω_n and ζ perturbations

Table 2. Modes obtained as eigenvalues of the coupled model, and their role in the design.

Mode	f_n (Hz)	ζ	Role
Drivetrain torsion	2.8500	0.0300	lightly damped; shaper target
Tower fore–aft (1st)	0.4493	0.0365	lightly damped; shaper target
Platform pitch	0.0513	0.3188	strongly aero-damped; *excluded* from the shaper

not an aero-hydro-servo-elastic one. All matrices, shaper instants and observer gains are in Appendices B–C, and Table 1 lists the settings; the same parameter set generates every number below.

4.1 Coupled model and identified modes

The eigenvalues of the coupled A give the three modes of Table 2; they are identified from the model, not imposed on it. The platform-pitch mode carries a damping ratio of 0.32, an order above the value a decoupled model produces, because collective pitch and the thrust dependence on relative wind damp it strongly — this is the physically expected behaviour of an operating FOWT and it drives the design conclusion below. All six input–output paths are non-zero: with T_g and β as inputs and ω_r, q_{fa}, θ_p as outputs, the largest numerator coefficients are 7.9×10^{-6}, 4.7×10^{2}, 4.0×10^{-7}, 2.1×10^{3}, 2.6×10^{-8} and 1.4×10^{2} respectively. Figure 1a shows the eigenvalue map and Fig. 1b the tower response to a generator-torque impulse, which is non-zero precisely because the model is coupled.

https://doi.org/10.5194/wes-2026-128
Preprint. Discussion started: 17 August 2026

Open Access
WIND ENERGY SCIENCE DISCUSSIONS

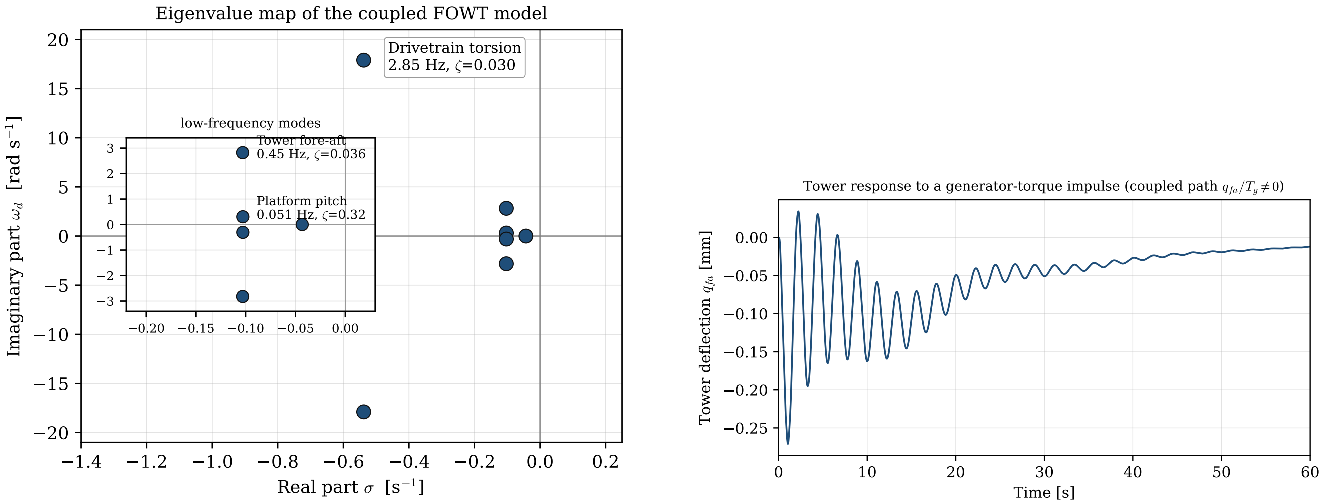

(a) Eigenvalue map (inset: low-frequency modes).

(b) Tower response to a torque impulse ($q_{fa}/T_g \neq 0$).

Figure 1. The coupled model: modes are identified from A, and the drivetrain reaches the structure.

Table 3. The design choice exposed by the coupled model. Percentages are reductions relative to the unshaped command.

	unshaped	3-mode shaper	**2-mode shaper**
Impulses / duration (s)	—	27 / 7.864	**9 / 0.860**
Tower-base FA DEL (MN m)	51.39	36.05 (−29.8 %)	**25.00** (**−51.4** %)
Platform-pitch DEL (MN m)	29.91	24.94 (−16.6 %)	29.75 (−0.6 %)
Peak tower deflection (mm)	36.2	41.5	**34.5**
Residual cancellation (with actuator) (%)	—	81.0	61.8
Peak out-of-band spillover max $\lvert\hat{S}\rvert$	1	19.24	**6.92**

4.2 Shaper synthesis and the design choice

Convolving the three single-mode UM shapers gives 27 impulses of amplitude ±1 over $7.864\,\mathrm{s}$, with $\sum_i A_i = 1.000000000000$ and residuals below 5×10^{-11} at all three modes, confirming Theorem 3.1 and Remark 3.2. The platform mode alone contributes $7.00\,\mathrm{s}$ of that duration. Because that mode is strongly damped it rings very little, so we also synthesize a two-mode shaper targeting only the drivetrain and tower: 9 impulses over $0.860\,\mathrm{s}$, cancelling both targets exactly and leaving $94.3\,\%$ at the platform. Figure 2a compares the two. Table 3 shows the outcome: the two-mode shaper is $9\times$ shorter and better on every metric except the platform load, which is small anyway. The three-mode shaper is worse than *no* shaping on peak deflection (41.5 versus $36.2\,\mathrm{mm}$), because its long, repeatedly reversing command injects more excursion than it cancels.

https://doi.org/10.5194/wes-2026-128
Preprint. Discussion started: 17 August 2026

WIND ENERGY SCIENCE DISCUSSIONS

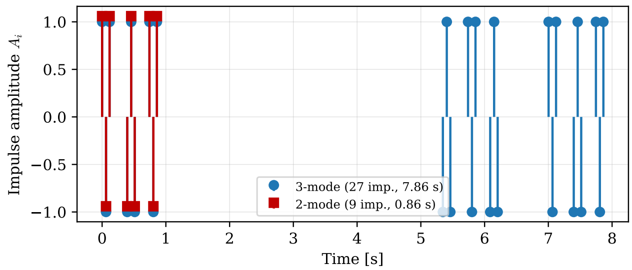

(a) Impulse trains.

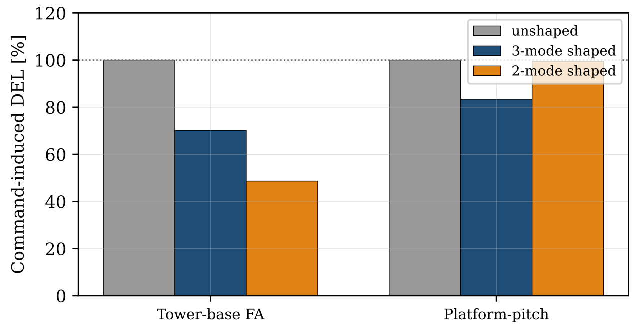

(b) Command-induced DEL.

Figure 2. Dropping the strongly damped platform mode shortens the shaper $9\times$ and improves the tower load.

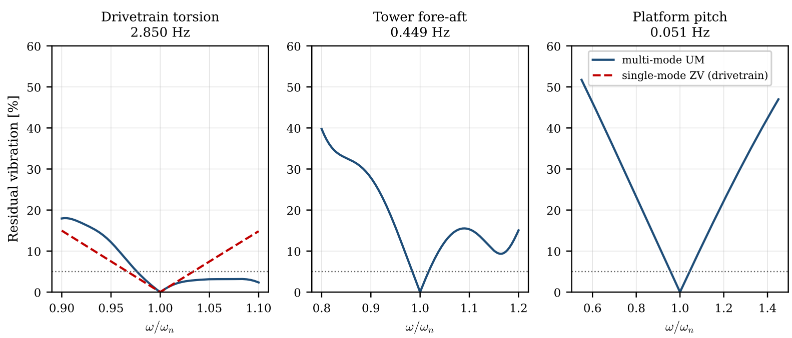

(a) Vibration sensitivity (exact residual).

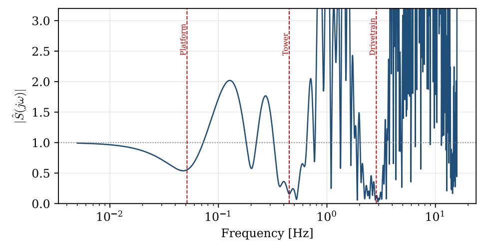

(b) Shaper spectrum.

Figure 3. Notches at the targets, and the out-of-band spillover that a ± 1 sequence necessarily carries.

4.3 Sensitivity and spillover

The sensitivity curves (Fig. 3a) reach zero at each targeted frequency. The shaper spectrum (Fig. 3b) shows the cost of a long ± 1 sequence: the three-mode shaper amplifies by up to 19.2 near $9.4\,\mathrm{Hz}$, well above the targets, whereas the two-mode shaper peaks at 6.9. Neither is unity out of band, so a command low-pass filter is advisable to avoid exciting dynamics that the design set omits; this is a further argument for the shorter sequence.

4.4 Perturbation, quantization and estimation error

Table 4 reports the actual residual against the bound of Proposition 3.3. The bound holds everywhere and is 2.3 to 38 times conservative, as Remark 3.4 anticipates. Quantizing the instants to the $10\,\mathrm{ms}$ command grid leaves $14.30\,\%$ at the drivetrain mode but only $0.68\,\%$ and $0.73\,\%$ at the tower and platform, a direct consequence of the weight $e^{a_\ell t_i}$; a $2\,\mathrm{ms}$ grid reduces the drivetrain figure to $1.76\,\%$. This is a concrete implementation requirement: shaping a $2.85\,\mathrm{Hz}$ mode needs a command grid

https://doi.org/10.5194/wes-2026-128
Preprint. Discussion started: 17 August 2026

Table 4. Residual under timing quantization: actual value and the bound of Proposition 3.3 (%).

Grid	Drivetrain (2.85 Hz)		Tower (0.449 Hz)		Platform (0.051 Hz)	
	actual	bound	actual	bound	actual	bound
2 ms	1.76	8.17	0.33	2.53	0.04	0.29
5 ms	5.66	22.38	1.53	6.75	0.23	0.77
10 ms	14.30	51.58	0.68	14.54	0.73	1.65

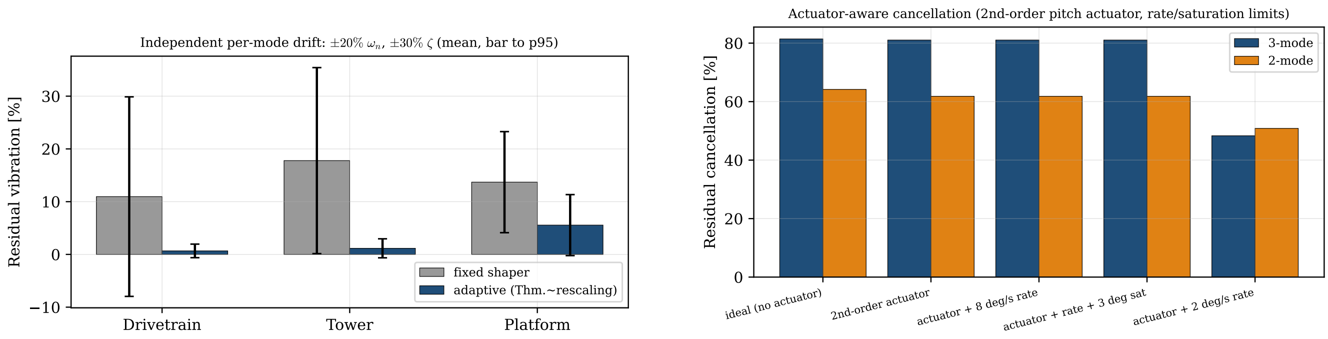

(a) Independent per-mode drift.

(b) Actuator-aware cancellation.

Figure 4. Adaptation recovers cancellation under frequency drift; a real pitch actuator does not destroy it, but a tight rate limit does.

several times faster than the loop rate, which is a further reason to prefer the two-mode design only if the drivetrain target is retained on a fast channel. A 2 % modal-frequency error leaves 3.4 % residual, against 6.5 % from Corollary 3.5.

4.5 Independent modal drift

Figure 4a reports 400 Monte-Carlo samples in which each mode's frequency and damping are perturbed *independently* by ±20 % and ±30 %. A fixed shaper leaves mean residuals of 10.4 %, 17.6 % and 13.3 % (95th percentiles up to 34.5 %). Rescaling by Theorem 3.7 reduces these to 0.66 %, 1.24 % and 6.00 %. When the damping is known exactly and only the frequency drifts, the residual is 0.00 % at every sample: the theorem is exactly what it claims and no more. The residual 6.00 % at the platform is the price of a ±30 % damping error on the mode whose damping is largest, and it is why the offline map $\varphi_i(\zeta)$ of Algorithm 1 is needed.

4.6 Actuator feasibility

The ideal shaped command demands a peak pitch rate of $200^\circ\,\mathrm{s}^{-1}$ and is not physically realizable. Passing it through the second-order actuator of Table 1 reduces the demand to $5.13^\circ\,\mathrm{s}^{-1}$, within the $8^\circ\,\mathrm{s}^{-1}$ limit, and — the useful result — barely

https://doi.org/10.5194/wes-2026-128
Preprint. Discussion started: 17 August 2026

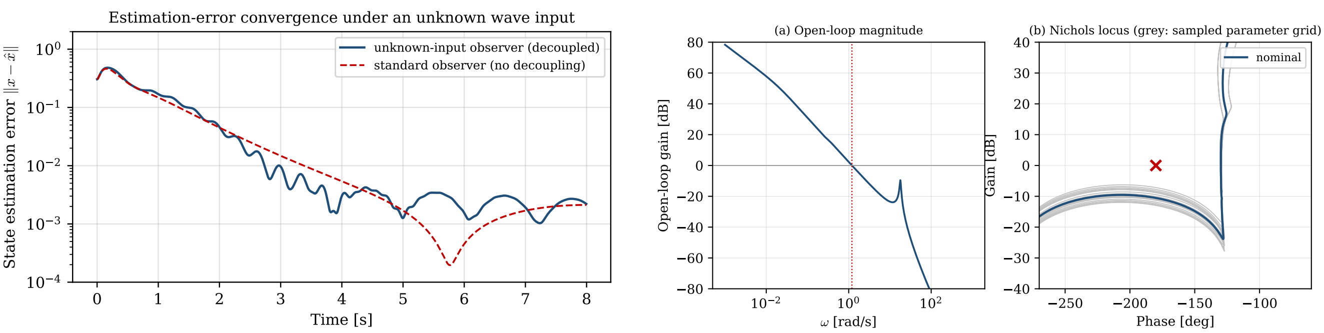

(a) Estimation-error convergence.

(b) Nominal feedback layer (illustrative).

Figure 5. The estimation layer, and the nominal fractional-order loop used to close the speed loop in the demonstration.

changes the cancellation, from $81.4\,\%$ to $81.0\,\%$ for the three-mode shaper and $64.2\,\%$ to $61.8\,\%$ for the two-mode one (Fig. 4b). The reason is that the actuator corner (1 Hz) lies well above the tower and platform modes being cancelled. Neither the $8^\circ\,\mathrm{s}^{-1}$ rate limit nor a $\pm 3^\circ$ travel limit binds. A tight $2^\circ\,\mathrm{s}^{-1}$ limit does bind and degrades the three-mode shaper to 48.3%, so rate authority, not the shaper, becomes the limiting factor. Because the impulses are command weights rather than actuator commands, the applied signal is the piecewise trajectory of the convolution, and its peak rate must be checked against the actuator specification as done here.

4.7 Estimation layer

For the four-channel sensor set the observability matrix of (A,C) has full rank 7, and after scaling the states to physically comparable ranges its singular values span 1.05×10^{-2} to 1.42×10^{5}, a condition number of 1.35×10^{7}: the realization is observable but poorly conditioned in one direction, which any implementation must respect. The unknown-input conditions hold, $\mathrm{rank}(CE) = \mathrm{rank}(E) = 1$, the decoupled pair (TA, C) is observable, and the decoupling identity $TE = 0$ is satisfied to machine precision. With the error poles of Appendix C the observer error settles to within $5\,\%$ of its initial value in $2.46\,\mathrm{s}$ under an unmodelled wave moment (Fig. 5a). We note honestly that a standard observer with the *same* assigned poles performs comparably in this model: the wave channel enters the platform equation through $1/I_p$, so the unknown input is small in state units and the advantage of decoupling is modest here. The value of Theorem 3.9 is the guarantee, which does not depend on the disturbance being small.

4.8 Nominal feedback layer

The shaping results above are feedforward and do not depend on the feedback design. For completeness the demonstration closes the rotor-speed loop with a fractional-order (CRONE-type) regulator $C(s) = K_c s^{-(\nu-1)}(s+\epsilon)/s$, $\nu = 1.45$, realized by a band-limited operator (Oustaloup et al., 2000; Sabatier et al., 2015; Podlubny, 1999). On the coupled channel it crosses over at $1.198\,\mathrm{rad\,s^{-1}}$ with a phase margin of 50.2°, a single positive-frequency gain crossing, all closed-loop poles in the open left

https://doi.org/10.5194/wes-2026-128
Preprint. Discussion started: 17 August 2026

half plane (maximal real part -0.034), a resonant peak of $2.29\,\mathrm{dB}$ and a modulus margin of 0.69 (Fig. 5b). Over the interval $\kappa \in [0.202, 15.63]$ on which $|L|$ is verified strictly decreasing, the margin stays within $[50.2°, 52.5°]$. We claim nothing more: this is a nominal, illustrative layer, robustness to structured FOWT parameter variation is *not* established here, and the loop is not part of the paper's contribution.

5 Limitations

The evidence should be read for exactly what it is. The model is a seven-state control-oriented reduction whose parameters are representative of the IEA 15 MW/VolturnUS-S system but were not identified from it; synthesis and evaluation therefore share a model, and the exact-cancellation results verify the theorems rather than establish turbine-level performance. The reported damage-equivalent loads are short-term, command-transition-induced values for the documented maneuver sequence; they are not lifetime or certification quantities, which would require the standardized design load cases, several wind speeds and sea states, and lifetime weighting (International Electrotechnical Commission, 2019). Shaping is feedforward: it removes command-induced excitation and does nothing about turbulence or waves, so it complements rather than replaces feedback. The modal identifier that Algorithm 1 presumes is specified but not validated here; Corollary 3.5 states the accuracy it must reach. Aerodynamic and hydrodynamic nonlinearities, blade and side–side modes, and sensor bias and drift in the integrated tower-top velocity are outside the model. The natural next step is cross-validation against high-fidelity aero-hydro-servo-elastic linearizations at several above-rated operating points, with the shaper designed on one model and tested on another.

6 Conclusion

This paper established the analytical cancellation and estimation properties of an adaptive multi-mode unity-magnitude shaping layer for floating offshore wind turbines and demonstrated its mechanisms on a coupled control-oriented model. Convolving single-mode UM shapers cancels every targeted mode exactly and preserves the commanded set-point; a non-asymptotic bound limits the residual under amplitude, timing and frequency-estimation error, and is measured to be 2.3 to 38 times conservative; rescaling the impulse instants by the estimated damped frequency restores exact cancellation under frequency drift, and is exactly that and no more, degrading gracefully when the damping also moves; and a full-order unknown-input observer supplies the states with proved decoupled convergence. The design result is the one a decoupled model conceals: because collective pitch damps the platform mode strongly, shaping it lengthens the sequence ninefold, worsens the peak deflection, triples the out-of-band spillover, and reduces the tower load by less. Shaping only the lightly damped modes gives a $0.86\,\mathrm{s}$, nine-impulse sequence that cuts the command-induced tower damage-equivalent load by $51.4\,\%$ and survives a realistic pitch actuator. The reported performance remains preliminary until validated on a dynamically coupled aero-hydro-servo-elastic model with realistic actuator and estimation constraints; within that scope, the message for floating-wind command design is simple — shape the modes that ring, and let the aerodynamics damp the rest.

https://doi.org/10.5194/wes-2026-128
Preprint. Discussion started: 17 August 2026

Appendix A: Single-mode UM instants

For a mode (ω_n,ζ) the UM shaper $A=[1,-1,1]$, $t=[0,t_2,t_3]$ solves $\mathcal{C}=\mathcal{S}=0$ of Lemma 2.2. In the undamped limit the conditions reduce to $1-\cos\varphi_2+\cos\varphi_3=0$ and $-\sin\varphi_2+\sin\varphi_3=0$ with $\varphi_i=\omega_d t_i$, whose solution is $\varphi_2=\pi/3$, $\varphi_3=2\pi/3$, i.e. $t_2=T/6$, $t_3=T/3$ with $T=2\pi/\omega_d$. For $\zeta>0$ the instants are computed numerically by continuation from that point. Over the damping interval used here, $\zeta\in[0.030,0.319]$, the continuation stayed on the same branch and the Jacobian of $(\mathcal{C},\mathcal{S})$ with respect to (t_2,t_3) remained non-singular; we do not claim uniqueness for all ζ. The full-precision normalized instants are

Mode	ζ	φ_2	φ_3
Drivetrain torsion	0.030040	1.101869113	2.094790677
Tower fore–aft	0.036490	1.113653681	2.094978945
Platform pitch	0.318775	1.634448089	2.141549795

giving $t=[0,\,0.061560364,\,0.117033934]\,\mathrm{s}$, $[0,\,0.394734708,\,0.742565589]\,\mathrm{s}$ and $[0,\,5.345506549,\,7.003996352]\,\mathrm{s}$ respectively. These are the values used by the code; the residuals below 5×10^{-11} quoted in Sect. 4 are obtained with the unrounded instants.

Appendix B: Numerical model

All quantities are in SI units: angles in rad, rates in $\mathrm{rad\,s^{-1}}$, tower deflection in m, torque in N m, pitch in rad, wave moment in N m. The state is $x=[\theta_{dt},\omega_r,\omega_g,q_{fa},\dot q_{fa},\theta_p,\dot\theta_p]^\top$, the input $u=[T_g,\beta]^\top$ and the disturbance $d=[V_w,M_{\mathrm{wave}}]^\top$.

$$A=\begin{bmatrix} 0 & 1 & -1 & 0 & 0 & 0 & 0\\ -9.7171 & -0.079433 & 0.032558 & 0 & -0.009375 & 0 & -1.4062\\ 310.95 & 1.0419 & -1.0419 & 0 & 0 & 0 & 0\\ 0 & 0 & 0 & 0 & 1 & 0 & 0\\ 0 & 0.41667 & 0 & -7.9944 & -0.20655 & 0 & -22.5\\ 0 & 0 & 0 & 0 & 0 & 0 & 1\\ 0 & 0.0034091 & 0 & 0 & -0.0012273 & -0.098696 & -0.20294 \end{bmatrix} \tag{B1}$$

$$B=\begin{bmatrix} 0 & 0\\ 0 & -0.1875\\ -1\times10^{-7} & 0\\ 0 & 0\\ 0 & -6.6667\\ 0 & 0\\ 0 & -0.054545 \end{bmatrix},\qquad E=\begin{bmatrix} 0 & 0\\ 0.009375 & 0\\ 0 & 0\\ 0 & 0\\ 0.15 & 0\\ 0 & 0\\ 0.0012273 & 4.5455\times10^{-11} \end{bmatrix} \tag{B2}$$

https://doi.org/10.5194/wes-2026-128
Preprint. Discussion started: 17 August 2026

eawe european academy of wind energy
Open Access WIND ENERGY SCIENCE DISCUSSIONS

$$C = \begin{bmatrix} 0 & 1 & 0 & 0 & 0 & 0 & 0 \\ 0 & 0 & 0 & 0 & 1 & 0 & 0 \\ 0 & 0 & 0 & 0 & 0 & 1 & 0 \\ 0 & 0 & 0 & 0 & 0 & 0 & 1 \end{bmatrix} \tag{B3}$$

The physical parameters are $J_r = 3.2\times10^8$, $J_g = 1\times10^7\,\mathrm{kg\,m^2}$, $k_{dt} = 3.109\times10^9\,\mathrm{N\,m\,rad^{-1}}$, $c_{dt} = 1.042\times10^7\,\mathrm{N\,m\,s}$, $L_t = 150\,\mathrm{m}$, $m_t = 1.2\times10^6\,\mathrm{kg}$, $k_t = 9.593\times10^6\,\mathrm{N\,m^{-1}}$, $c_t = 6.786\times10^4\,\mathrm{N\,s\,m^{-1}}$, $I_p = 2.2\times10^{10}\,\mathrm{kg\,m^2}$, $K_{hs} = 2.171\times10^9\,\mathrm{N\,m\,rad^{-1}}$, $B_{vis} = 4.147\times10^8\,\mathrm{N\,m\,s}$, and the aerodynamic partial derivatives at the above-rated operating point ($\omega_{r0} = 0.792\,\mathrm{rad\,s^{-1}}$) are $g_\omega = -1.5\times10^7$, $g_\beta = -6\times10^7$, $g_V = 3\times10^6$, $k_\omega = 5\times10^5$, $k_\beta = -8\times10^6$, $k_V = 1.8\times10^5$ in SI units.

The rotor-speed/generator-torque channel of the coupled model is $G(s) = \omega_r(s)/T_g(s) = \mathrm{num}\,G/\mathrm{den}\,G$ with

$$\begin{aligned} \mathrm{num}\,G = [&0,\ 3.1086\times10^{-15},\ -3.2564\times10^{-9},\ -9.7304\times10^{-7},\ -4.2431\times10^{-7}, \\ &-7.8834\times10^{-6},\ -1.5989\times10^{-6},\ -7.6669\times10^{-7}], \\ \mathrm{den}\,G = [&1,\ 1.5308,\ 329.29,\ 156.65,\ 2611.5,\ 646.06,\ 289.03,\ 11.5]. \end{aligned} \tag{B4}$$

The nominal fractional-order feedback layer of Sect. 4 is the band-limited realization of $C(s) = K_c\, s^{-(\nu-1)}(s+\epsilon)/s$ with $\nu = 1.45$ and $\epsilon = 0.05$, on $[\omega_{cg}/60,\, 60\omega_{cg}]$ with $2N+1 = 11$ cells and $\omega_{cg} = 1.2\,\mathrm{rad\,s^{-1}}$. Its rational form, in SI units ($\mathrm{rad\,s^{-1}}$ in, $\mathrm{N\,m}$ out), has

$$\begin{aligned} \mathrm{num}\,C = [&4.2667\times10^{8},\ 4.7691\times10^{10},\ 1.7170\times10^{12},\ 2.5477\times10^{13},\ 1.6906\times10^{14}, \\ &5.1920\times10^{14},\ 7.5028\times10^{14},\ 5.1547\times10^{14},\ 1.6995\times10^{14},\ 2.7143\times10^{13}, \\ &2.1028\times10^{12},\ 7.5540\times10^{10},\ 1.0005\times10^{9}], \end{aligned} \tag{B5}$$

$$\begin{aligned} \mathrm{den}\,C = [&6.8517,\ 547.60,\ 1.4090\times10^{4},\ 1.4926\times10^{5},\ 7.0558\times10^{5},\ 1.5365\times10^{6},\ 1.5595\times10^{6}, \\ &7.3767\times10^{5},\ 1.6074\times10^{5},\ 1.5631\times10^{4},\ 625.77,\ 8.0654,\ 0]. \end{aligned} \tag{B6}$$

These coefficients give $|C(j\omega_{cg})G(j\omega_{cg})| = 1.0000$ directly, with no further normalization; the loop is $L = -CG$, the minus sign carrying the negative-feedback convention of the torque channel.

https://doi.org/10.5194/wes-2026-128
Preprint. Discussion started: 17 August 2026

Open Access
WIND ENERGY SCIENCE
DISCUSSIONS

Appendix C: Observer coefficients

The unknown-input observer of Theorem 3.9 is designed on the coupled model with the unknown input taken as the wave-moment channel. The assigned error poles are $\{-2, -2.5, -3, -3.5, -4, -4.5, -5\}\,\mathrm{s}^{-1}$, giving

$$H = \begin{bmatrix} 0 & 0 & 0 & 0 \\ 0 & 0 & 0 & 0 \\ 0 & 0 & 0 & 0 \\ 0 & 0 & 0 & 0 \\ 0 & 0 & 0 & 0 \\ 0 & 0 & 0 & 0 \\ 0 & 0 & 0 & 1 \end{bmatrix} \tag{C1}$$

310

$$K_1 = \begin{bmatrix} 29.462 & 0.0033186 & 0.38863 & 0.38863 \\ 9.3787 & -0.01391 & -0.54477 & -1.951 \\ -298.02 & 0.13956 & 16.836 & 16.836 \\ 1.9413\times10^{-6} & -0.40724 & 1.6337\times10^{-7} & 1.6337\times10^{-7} \\ 0.41666 & 6.7935 & -7.5144\times10^{-7} & -22.5 \\ -1.5347\times10^{-5} & -3.0363\times10^{-8} & 3.5 & 0.50001 \\ -1.5347\times10^{-5} & -3.0363\times10^{-8} & -0.49999 & 3.5 \end{bmatrix} \tag{C2}$$

$$K = \begin{bmatrix} 29.462 & 0.0033186 & 0.38863 & 0 \\ 9.3787 & -0.01391 & -0.54477 & -1.4062 \\ -298.02 & 0.13956 & 16.836 & 0 \\ 1.9413\times10^{-6} & -0.40724 & 1.6337\times10^{-7} & 0 \\ 0.41666 & 6.7935 & -7.5144\times10^{-7} & -22.5 \\ -1.5347\times10^{-5} & -3.0363\times10^{-8} & 3.5 & 1 \\ -1.5347\times10^{-5} & -3.0363\times10^{-8} & -0.49999 & 0 \end{bmatrix} \tag{C3}$$

with $T = I - HC$ and $F = TA - K_1C$ Hurwitz ($\max \Re\lambda(F) = -2.000\,\mathrm{s}^{-1}$). The standard observer used for comparison uses
315 the same assigned poles.

Code and data availability. The model, shaper, observer and figure-generation scripts, the parameter files and the random seeds reproduce every number and figure in this paper and are available from the corresponding author on reasonable request. They are not deposited in a public repository because they form part of a larger in-house simulation framework that is still under active development and is not documented or packaged for standalone distribution; the authors therefore provide a working, correctly parameterized version, together with

https://doi.org/10.5194/wes-2026-128
Preprint. Discussion started: 17 August 2026

320 the instructions needed to run it, to anyone who asks. All quantities required to reproduce the study independently — the model matrices, the shaper impulse instants and the observer gains — are reported in Appendices A–C. The reference turbine and platform definitions are public (Gaertner et al., 2020; Allen et al., 2020).

Author contributions. A. Mseddi: conceptualization, methodology, writing. I. Bouzida: formal analysis, validation. O. Naifar: methodology, supervision, writing–review. All authors approved the final manuscript.

325 *Competing interests.* The authors declare no competing interests.

Financial support. This research received no specific grant from any funding agency.

https://doi.org/10.5194/wes-2026-128
Preprint. Discussion started: 17 August 2026

References

Abbas, N. J., Zalkind, D. S., Pao, L., and Wright, A.: A reference open-source controller for fixed and floating offshore wind turbines, Wind Energy Science, 7, 53–73, https://doi.org/10.5194/wes-7-53-2022, 2022.

Abid, A., Jallouli-Khlif, R., Derbel, N., and Melchior, P.: Synthesis of unity magnitude shaper: Extension for explicit fractional derivative systems, in: 2016 13th International Multi-Conference on Systems, Signals & Devices (SSD), pp. 108–113, https://doi.org/10.1109/ssd.2016.7473746, 2016.

Allen, C., Viscelli, A., Dagher, H., Goupee, A., Gaertner, E., Abbas, N., Hall, M., and Barter, G.: Definition of the UMaine VolturnUS-S Reference Platform Developed for the IEA Wind 15-Megawatt Offshore Reference Wind Turbine, Tech. rep., Office of Scientific and Technical Information (OSTI), https://doi.org/10.2172/1660012, 2020.

Alshaya, A.: Vibration control of flexible dynamic systems using smooth robust input shapers: theory and application, International Journal of Dynamics and Control, 13, https://doi.org/10.1007/s40435-025-01803-6, 2025.

Aslmostafa, E., Mirzaei, M., Hamida, M., and Plestan, F.: Experimental evaluation of robust nonlinear control strategies for regions II and III for floating offshore wind turbines, Ocean Engineering, 346, 123 887, https://doi.org/10.1016/j.oceaneng.2025.123887, 2026.

Bai, H., Xu, K., and Gao, Z.: Development and Future Challenges of Offshore Floating Wind Turbine Technologies in China, Engineering, https://doi.org/10.1016/j.eng.2026.01.006, 2026.

Darouach, M., Zasadzinski, M., and Xu, S.: Full-order observers for linear systems with unknown inputs, IEEE Transactions on Automatic Control, 39, 606–609, https://doi.org/10.1109/9.280770, 1994.

Gaertner, E., Rinker, J., Sethuraman, L., Zahle, F., Anderson, B., Barter, G., Abbas, N., Meng, F., Bortolotti, P., Skrzypinski, W., Scott, G., Feil, R., Bredmose, H., Dykes, K., Shields, M., Allen, C., and Viselli, A.: IEA Wind TCP Task 37: Definition of the IEA 15-Megawatt Offshore Reference Wind Turbine, Tech. rep., Office of Scientific and Technical Information (OSTI), https://doi.org/10.2172/1603478, 2020.

Gürleyük, S. S.: Optimal unity-magnitude input shaper duration analysis, Archive of Applied Mechanics, 77, 63–71, https://doi.org/10.1007/s00419-006-0080-2, 2006.

Hawari, Q., Kim, T., Ward, C., and Fleming, J.: LQG control for hydrodynamic compensation on large floating wind turbines, Renewable Energy, 205, 1–9, https://doi.org/10.1016/j.renene.2023.01.067, 2023.

Hummel, J. I. S., Kober, J., and Mulders, S. P.: Output-constrained individual pitch control methods using the multiblade coordinate transformation: trading off actuation effort and blade fatigue load reduction for wind turbines, Wind Energy Science, 10, 2005–2023, https://doi.org/10.5194/wes-10-2005-2025, 2025.

International Electrotechnical Commission: IEC 61400-1:2019 Wind energy generation systems – Part 1: Design requirements, International Standard, 4th edition, Geneva, Switzerland, 2019.

Jonkman, J. M. and Matha, D.: Dynamics of offshore floating wind turbines—analysis of three concepts, Wind Energy, 14, 557–569, https://doi.org/10.1002/we.442, 2011.

Larsen, T. J. and Hanson, T. D.: A method to avoid negative damped low frequent tower vibrations for a floating, pitch controlled wind turbine, Journal of Physics: Conference Series, 75, 012 073, https://doi.org/10.1088/1742-6596/75/1/012073, 2007.

Liu, J., Cai, C., Song, D., Zheng, J., Guo, X., Sun, X., Hu, Z., and Li, Q.: Power output and platform motion regulation of floating offshore wind turbine using model predictive control based on coupled dynamics model, Ocean Engineering, 322, 120 451, https://doi.org/10.1016/j.oceaneng.2025.120451, 2025.

Mseddi, A., Abid, A., Naifar, O., Rhaima, M., Ben Makhlouf, A., and Mchiri, L.: Investigation of the Robust Fractional Order Control Approach Associated with the Online Analytic Unity Magnitude Shaper: The Case of Wind Energy Systems, Fractal and Fractional, 8, 187, https://doi.org/10.3390/fractalfract8040187, 2024.

Oustaloup, A., Levron, F., Mathieu, B., and Nanot, F.: Frequency-band complex noninteger differentiator: characterization and synthesis, IEEE Transactions on Circuits and Systems I: Fundamental Theory and Applications, 47, 25–39, https://doi.org/10.1109/81.817385, 2000.

Podlubny, I.: Fractional-order systems and $PI^{\lambda}D^{\mu}$-controllers, IEEE Transactions on Automatic Control, 44, 208–214, https://doi.org/10.1109/9.739144, 1999.

Poty, A., Melchior, P., Levron, F., Orsoni, B., and Oustaloup, A.: Preshaping command inputs for explicit fractional derivative systems: Application to CRONE control, in: 2003 European Control Conference (ECC), pp. 2279–2284, https://doi.org/10.23919/ecc.2003.7085306, 2003.

Pustina, L., Lugni, C., Bernardini, G., Serafini, J., and Gennaretti, M.: Control of power generated by a floating offshore wind turbine perturbed by sea waves, Renewable and Sustainable Energy Reviews, 132, 109 984, https://doi.org/10.1016/j.rser.2020.109984, 2020.

Pustina, L., Serafini, J., Pasquali, C., Solero, L., Lidozzi, A., and Gennaretti, M.: A novel resonant controller for sea-induced rotor blade vibratory loads reduction on floating offshore wind turbines, Renewable and Sustainable Energy Reviews, 173, 113 073, https://doi.org/10.1016/j.rser.2022.113073, 2023.

Pustina, L., Biral, F., Bertolazzi, E., and Serafini, J.: A multi-objective economic nonlinear model predictive controller for power and platform motion on floating offshore wind turbines, Ocean Engineering, 342, 122 888, https://doi.org/10.1016/j.oceaneng.2025.122888, 2025.

Sabatier, J., Lanusse, P., Melchior, P., and Oustaloup, A.: Fractional Order Differentiation and Robust Control Design, Springer Netherlands, https://doi.org/10.1007/978-94-017-9807-5, 2015.

Singer, N. C. and Seering, W. P.: Preshaping Command Inputs to Reduce System Vibration, Journal of Dynamic Systems, Measurement, and Control, 112, 76–82, https://doi.org/10.1115/1.2894142, 1990.

Singhose, W.: Command shaping for flexible systems: A review of the first 50 years, International Journal of Precision Engineering and Manufacturing, 10, 153–168, https://doi.org/10.1007/s12541-009-0084-2, 2009.